
FLEXI-NEURA: A CONFIGURABLE NEUROMORPHIC ACCELERATOR WITH ADAPTIVE BIT-PRECISION EXPLORATION FOR EDGE SNNs

A PREPRINT

✉ **Mohammad Farahani**

High Performance Embedded Architecture Lab.
School of Electrical and Computer Engineering
College of Engineering, University of Tehran
Tehran, Iran
farahani.mohammad@ut.ac.ir

✉ **Mohammad Rasoul Roshanshah**

High Performance Embedded Architecture Lab.
School of Electrical and Computer Engineering
College of Engineering, University of Tehran
Tehran, Iran
mrroshanshah@ut.ac.ir

Saeed Safari

High Performance Embedded Architecture Lab.
School of Electrical and Computer Engineering
College of Engineering, University of Tehran
Tehran, Iran
saeed@ut.ac.ir

ABSTRACT

Neuromorphic accelerators promise unparalleled energy efficiency and computational density for spiking neural networks (SNNs), especially in edge intelligence applications. However, most existing platforms exhibit rigid architectures with limited configurability, restricting their adaptability to heterogeneous workloads and diverse design objectives. To address these limitations, we present Flexi-NeurA—a parameterizable neuromorphic accelerator (core) that unifies configurability, flexibility, and efficiency. Flexi-NeurA allows users to customize neuron models, network structures, and precision settings at design time. By pairing these design-time configurability and flexibility features with a time-multiplexed and event-driven processing approach, Flexi-NeurA substantially reduces the required hardware resources and total power while preserving high efficiency and low inference latency. Complementing this, we introduce Flex-plorer, a heuristic-guided design-space exploration (DSE) tool that determines cost-effective fixed-point precisions for critical parameters—such as decay factors, synaptic weights, and membrane potentials—based on user-defined trade-offs between accuracy and resource usage. Based on the configuration selected through the Flex-plorer process, RTL code is configured to match the specified design. Comprehensive evaluations across MNIST, SHD, and DVS benchmarks demonstrate that the Flexi-NeurA and Flex-plorer co-framework achieves substantial improvements in accuracy, latency, and energy efficiency. A three-layer 256–128–10 fully connected network with LIF neurons mapped onto two processing cores achieves 97.23% accuracy on MNIST with 1.1 ms inference latency, utilizing only 1,623 logic cells, 7 BRAMs, and 111 mW of total power—establishing Flexi-NeurA as a scalable, edge-ready neuromorphic platform.

Keywords Neuromorphic hardware · Spiking neural networks · Configurable hardware · Edge-AI · Precision optimization · Design-space exploration

1 Introduction

Edge AI is the practice of executing AI models at or near the location where data is generated rather than relying only on distant cloud infrastructure [1]. Keeping computation close enables the qualities that edge systems care about

most—low latency and low bandwidth usage improving privacy—since physical proximity to data sources confers these benefits [2]. Since edge devices are resource- and energy-constrained, practical edge-AI must be power-efficient while still delivering low-latency inference.

Artificial Neural Networks (ANNs) underpin edge-AI, but to be viable on edge devices they must be engineered for low power and low latency: unoptimized DNNs are too compute-heavy for hardware, and inference can impose intolerable latency and energy overheads [3].

Spiking Neural Networks (SNNs) are brain-inspired, event-driven models that update only on arriving spikes, representing signals as time-coded binary spike trains [4], [5], [6]. Their sparse spatiotemporal activity engages compute and memory only on events, reducing arithmetic and memory traffic, yielding high energy efficiency and low latency [7]. This directly matches edge-AI constraints: by computing and communicating only when spikes occur, SNNs deliver low power and low latency inference at the edge [8]. Hardware acceleration further improves throughput and efficiency for real-time SNNs on constrained devices by mapping event-driven workloads onto parallel computing resources [9].

Designing efficient neuromorphic hardware requires addressing key challenges such as the need for flexible configurations to support diverse neuron models and network topologies, as seen in Spiker+ [10]. Event-driven processing, as implemented in ODIN [11], ReckOn [12], and Morpich [13], ensures energy efficiency by activating only upon relevant spikes, reducing unnecessary computations. Time multiplexing, demonstrated in Loihi [14] and Morpich, optimizes resource usage, enabling efficient scaling. The ability to apply mixed-precision to parameters, seen in Loihi, balances accuracy and resource consumption. Multi-core processing in Morpich enhances parallelism, improving throughput. Efficient memory organization in Loihi and ReckOn minimizes data movement, enhancing performance. Finally, Design Space Exploration (DSE) tools such as SpikeExplorer [15] for Spiker+ optimize hardware configurations, to ensure that accelerators meet specific application requirements. These features are essential for addressing real-world challenges in SNN hardware.

Motivated by the need for architectural flexibility in edge-oriented SNN acceleration, we present Flexi-NeurA, a configurable neuromorphic processing core that exposes key design choices as pre-synthesis parameters. Flexi-NeurA enables designers to select the network topology, neuron model, and numerical precision of synaptic weights, membrane potentials, and synaptic currents prior to hardware generation. By elevating these choices to design time, the hardware is specialized to the target application, instantiating only the required functional units and allocating memory according to network size and precision, thereby avoiding unnecessary logic and reducing resource usage.

Flexi-NeurA employs an event-driven and time-multiplexed execution model in which neuron computation is sequentially reused across neurons, significantly lowering area and power consumption while maintaining realtime inference capability. Network layers are mapped onto a multi-core architecture, where each core implements a single layer and can be configured independently, enabling heterogeneous layer designs within the same system.

This architectural flexibility results in a large design space in which different accuracy-hardware trade-offs can be realized. To efficiently navigate this space, we introduce Flex-plorer, a software framework that performs precision-aware design-space exploration. Flex-plorer takes user-defined constraints, trains the target SNN, and applies simulated annealing to identify low-cost configurations within the specified bounds. Based on the selected configuration, it generates the corresponding RTL, high-level driver, and encoded datasets, enabling direct deployment and reproducible evaluation.

The main contributions of this work are summarized as follows:

- A design-time configurable, event-driven, time-multiplexed, multi-core SNN accelerator that supports multiple neuron models, network topologies, and precision settings.
- A precision-aware design-space exploration framework that automatically identifies application-specific, cost-effective hardware configurations using simulated annealing.

The rest of the paper is organized as follows: Section 1 introduces the problem, motivation, and contributions; Section 2 reviews SNN basics and edge needs; Section 3 surveys accelerators and DSE; Section 4 presents Flexi-NeurA; Section 5 describes Flex-plorer and the cost model; Section VI reports results and comparisons; Section 6 concludes.

2 Background

This section reviews the essential SNN background needed for the rest of the paper.

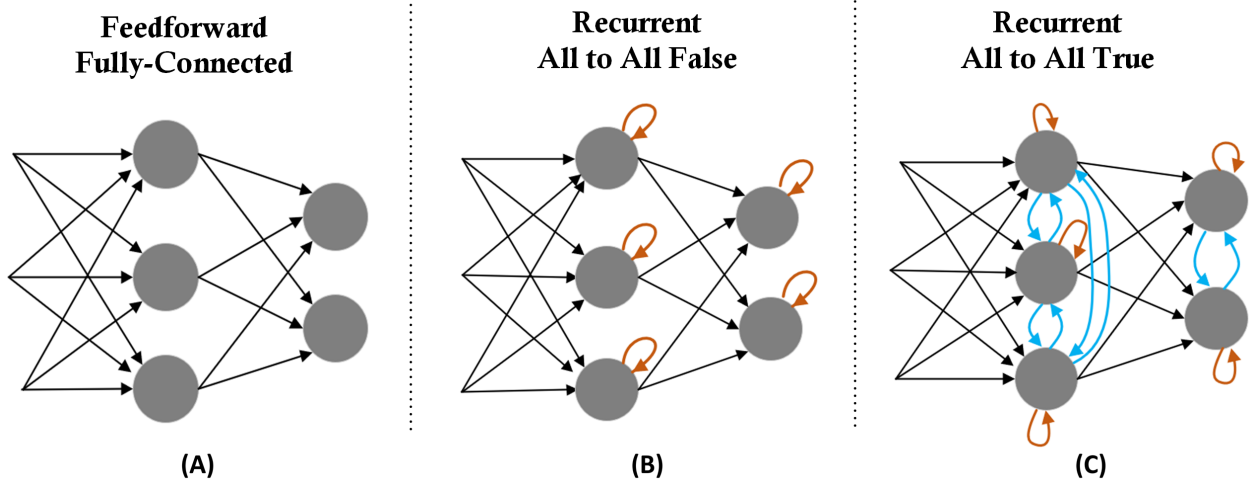


Figure 1: Spiking neural network topologies: (A) Fully-connected Feedforward, (B) Recurrent All-to-All False, and (C) Recurrent All-to-All.

2.1 Spiking Neural Networks

SNNs encode information as discrete spikes (rather than continuous activations), so computation is event- and time-based, driven by the timing of the spikes. Implementations range from analog to digital; here, we focus on digital SNNs, where a spike is a binary event (1/0), and neurons act as compact modules exchanging these event streams.

Neuronal connectivity in SNNs spans a wide range of diverse network topologies—from feedforward to recurrent architectures. Recurrent designs include reservoir networks with irregular, probabilistic synaptic connections [16], as well as structured recurrent networks that follow regular connection patterns.

Within the range of spiking network topologies, Flexi-NeurA supports three implementations: Fully-connected Feedforward (FF); recurrent with All-to-All False (ATA-F); and recurrent with All-to-All True (ATA-T), all based on SNN-Torch [17]. Each mode can be selected per layer at design time to match application needs.

Fully-connected feedforward (FF) networks propagate activity strictly from earlier layers to later ones, with no recurrent feedback (Fig. 1A). In each layer, every neuron is connected via synapses to all neurons in the immediately preceding layer.

Recurrent All-to-All False (ATA-F) adds temporal memory at low cost by avoiding dense intra-layer recurrence: In this architecture, recurrence is limited to self-feedback (Fig. 1B), so complexity and power consumption remain lower than in fully recurrent designs. In ATA-F, each neuron connects to all neurons in the previous layer and also to its own past output (self-loop). At each time step, it processes all incoming spikes from the previous layer and uses its own output from the prior step as an additional feedback input.

Recurrent All-to-All True (ATA-T) networks increase temporal memory by using dense intra-layer feedback. At each time step, every neuron receives feedforward spikes from all neurons in the preceding layer, as well as recurrent inputs from the previous time step consisting of its own output and the outputs of all neurons in the same layer; the topology is illustrated in Fig. 1C for plausibility.

2.2 Neuron Models

Computational neuroscience offers a spectrum of neuron models grounded in membrane-conductance data and formal modeling: while the Hodgkin–Huxley model achieves high biophysical fidelity at substantial computational cost [18], [19], [20], The Izhikevich model reduces complexity while preserving key spiking behaviors. For hardware—especially at the edge—the LIF and its derivatives (IF, synaptic) are most practical, maintaining acceptable biological plausibility while mapping efficiently to compact, low-power hardware implementations [21].

Before deriving the neuron models, we define the key terms: At each time step, the $I_{in}(t)$ input current is the sum of all spikes received in that step, each scaled by its synaptic weight; depending on the topology, these spikes may come from the previous layer, from the neuron’s own output one step earlier (self-feedback), and/or from same-layer neurons one step earlier. Temporal integration occurs in the $I_{syn}(t)$ synaptic current, the $U(t)$ membrane potential, or both,

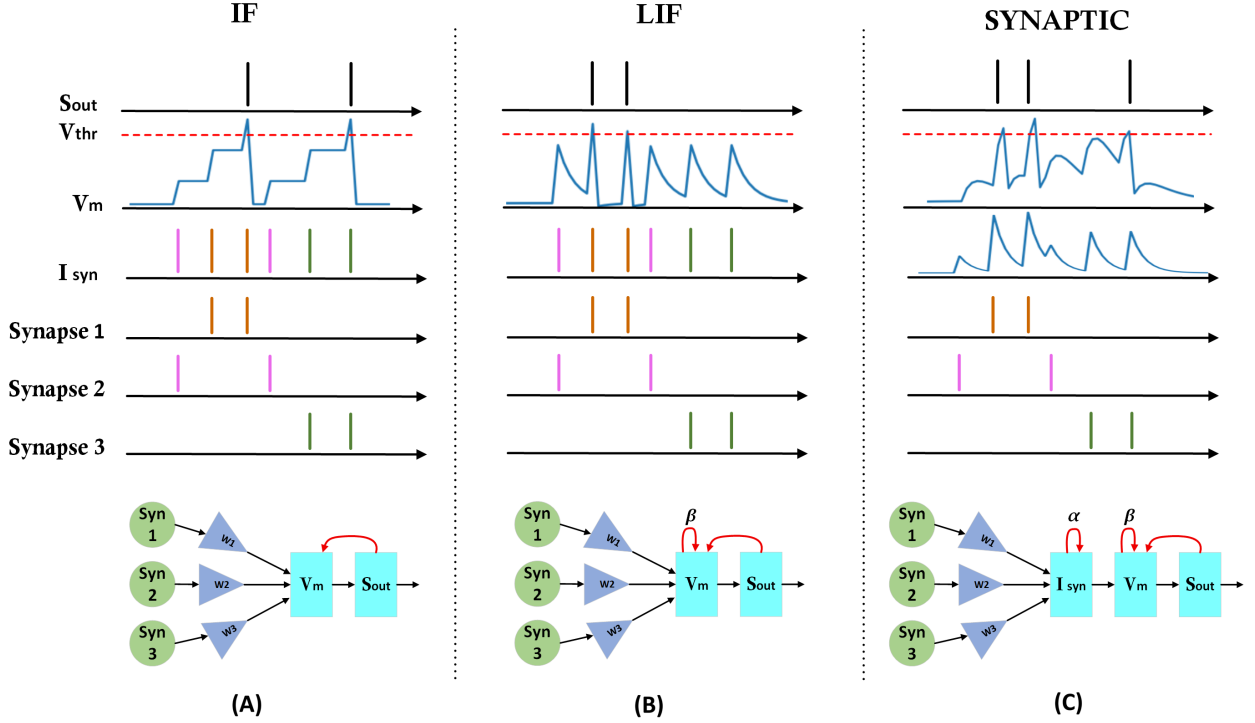


Figure 2: Spiking neuron models: (A) IF (B) LIF (C) Synaptic.

depending on the neuron model. A spike is generated ($S[t + 1] = 1$) when the membrane potential exceeds its U_{thr} threshold, and this firing is recorded in the next time step. Both membrane and synaptic states leak every step; the leak factors—beta for the membrane and alpha for the synapse—set how much of each state is retained versus lost, with $\alpha, \beta \in (0, 1)$ (i.e., both strictly between 0 and 1). After a spike, the reset rule updates the membrane potential either by setting it to zero (reset to zero) or by subtracting the threshold from its value (reset by subtract).

We now examine the equations of the three neuron models, based on SNN-Torch, a framework for SNNs. As shown in Fig. 2, each model receives three synapses driven by the same spike patterns, allowing a fair, side-by-side comparison of parameters and dynamics. You can refer to the figure while reading each model to see the corresponding input and output spike traces:

Based on Eq. 1, the IF neuron (with no leakage) updates its membrane potential by adding the input current of the current step to the previous potential and subtracting the reset term when a spike occurs — as shown in Fig. 2A. The input current is the weighted sum of all presynaptic spikes received in that step. If the updated potential exceeds the threshold U_{thr} , the neuron fires at the next step and the reset operator R is applied (e.g., reset-to-zero or reset-by-subtract); otherwise, the potential simply persists to the next step without leakage.

$$U[t + 1] = U[t] + I_{\text{in}}[t + 1] - R \quad (1)$$

LIF model (Eq. 2): the step’s input current I_{in} is the weighted sum of synapses that spiked in that step; as depicted in Fig. 2B, the membrane potential U combines this I_{in} with a leaky carryover of the previous U ; if the result exceeds U_{thr} , the neuron fires and the reset rule is applied. Otherwise, U decays by the leak factor β and is carried to the next step.

$$U[t + 1] = \beta U[t] + I_{\text{in}}[t + 1] - R \quad (2)$$

In the synaptic neuron model (Eq. 3), the input current I_{in} is computed at each time step as the weighted sum of all spikes received in that step. As shown in Fig. 2C, the synaptic current I_{syn} is then updated by adding I_{in} while retaining only a fraction α of its previous value—this leak occurs every step, regardless of spiking. Next, the membrane potential U keeps a fraction β of its prior value and adds the updated I_{syn} ; if the result exceeds U_{thr} , the neuron fires at the next step and the reset rule is applied, otherwise U continue to decay with β , respectively.

$$\begin{aligned} I_{syn}[t+1] &= \alpha I_{syn}[t] + I_{in}[t+1] \\ U[t+1] &= \beta U[t] + I_{syn}[t+1] - R \end{aligned} \quad (3)$$

3 Related Work

Neuromorphic accelerators are essential for efficient spiking neural network (SNN) computation, and digital designs have emerged as prominent solutions. These accelerators can be categorized into FPGA-based and ASIC-based platforms, each offering unique advantages depending on their focus on flexibility, performance, and power efficiency.

Among the ASIC-based accelerators, Intel Loihi [14] is a highly efficient chip that focuses on event-driven computation with fine-grained parallelism, making it ideal for large-scale SNNs requiring low power and real-time operation. IBM TrueNorth [22], on the other hand, is optimized for ultra-dense, low-leakage cores designed for inference tasks, focusing on scalability, low power, and efficient processing for large SNNs. ODIN [11], another ASIC-based processor, targets low-power event-driven computation and supporting flexible neuron models. MorphIC [13] is designed for low-power embedded applications, utilizing multi-core architecture to enable flexible, event-driven computation with highly efficient resource usage. ReckOn [12] is an ASIC-based accelerator focused on low-power, real-time processing with event-driven computation. It features a multi-core architecture for scalable, parallel processing, optimizing resource usage and energy efficiency for edge applications. NEXUS [23], leveraging a 16-core architecture and a diamond NoC topology, is optimized for energy-efficient real-time data processing, particularly in small-scale SNNs for edge devices with constrained resources.

Finally, FPGA implementations emphasize flexibility and low-power consumption, making them suitable for edge and embedded applications with tight power and resource budgets. Spiker+ [10] is optimized for low-power and clock-driven computation, offering flexibility in network topology and customizable neuron models, making it ideal for a variety of SNN tasks. Similarly, Han et al. [24] focuses on low-power, event-driven computation using a hybrid updating algorithm that combines time-stepped and event-driven methods, optimizing both performance and energy efficiency for real-time edge applications. Li et al. [25] introduces an implementation with an adaptive clock/event-driven scheme that dynamically switches between clock-driven and event-driven computation, further enhancing power efficiency for resource-constrained edge devices. These platforms provide customizable neuron models and topologies, enabling efficient handling of diverse SNN tasks while optimizing resource consumption.

SpikeExplorer [15] is a design space exploration tool specifically optimized for the Spiker+ accelerator. It automates the selection of key parameters such as accuracy, power consumption, and latency, enabling efficient hardware configurations. The tool uses Bayesian optimization to streamline the design process, ensuring energy-efficient solutions for edge applications while minimizing resource usage.

4 Proposed Hardware

The Flexi-NeurA processing core is composed of four modular subunits: an SPI Slave, a Controller, a Configurable Neuron Unit (CNU), and an AER Management Unit (AMU), which together provide fine-grained architectural flexibility (Fig. 3). This modular organization enables support for multiple neuron models and network topologies while optimizing hardware utilization, reducing power consumption, and enabling real-time inference. By instantiating only the components required by a given configuration, the architecture achieves high area and energy efficiency.

Flexi-NeurA is built around four key architectural principles: time-multiplexed computation, event-driven operation, multi-core scalability, and design-time configurability.

Neuron updates in Flexi-NeurA follow a time-multiplexed execution model in which a shared neuron-compute datapath sequentially processes all neurons in a layer. For each neuron, the datapath integrates incoming spikes into the membrane potential or synaptic current, evaluates threshold crossing or leakage, and then proceeds to the next neuron. This sequential reuse of compute resources significantly reduces hardware overhead while preserving deterministic execution.

Computation is triggered exclusively by spike events, which are encoded as address-based event packets. Four packet types are employed. The Address of Spike in Previous Layer (ASPL) is a 9-bit packet generated upon neuron firing that carries the source neuron address and a control bit. The Address of Spike in Current Layer (ASCL) is an 8-bit packet used in recurrent networks to convey intra-layer spike information for the next time step. The End of Time Step (EOTS) is a 9-bit control packet indicating the completion of all spike events for a time step. The End of Input (EOIN) is a 9-bit packet signaling the end of an input sequence and initiating neuron reset and leakage evaluation.

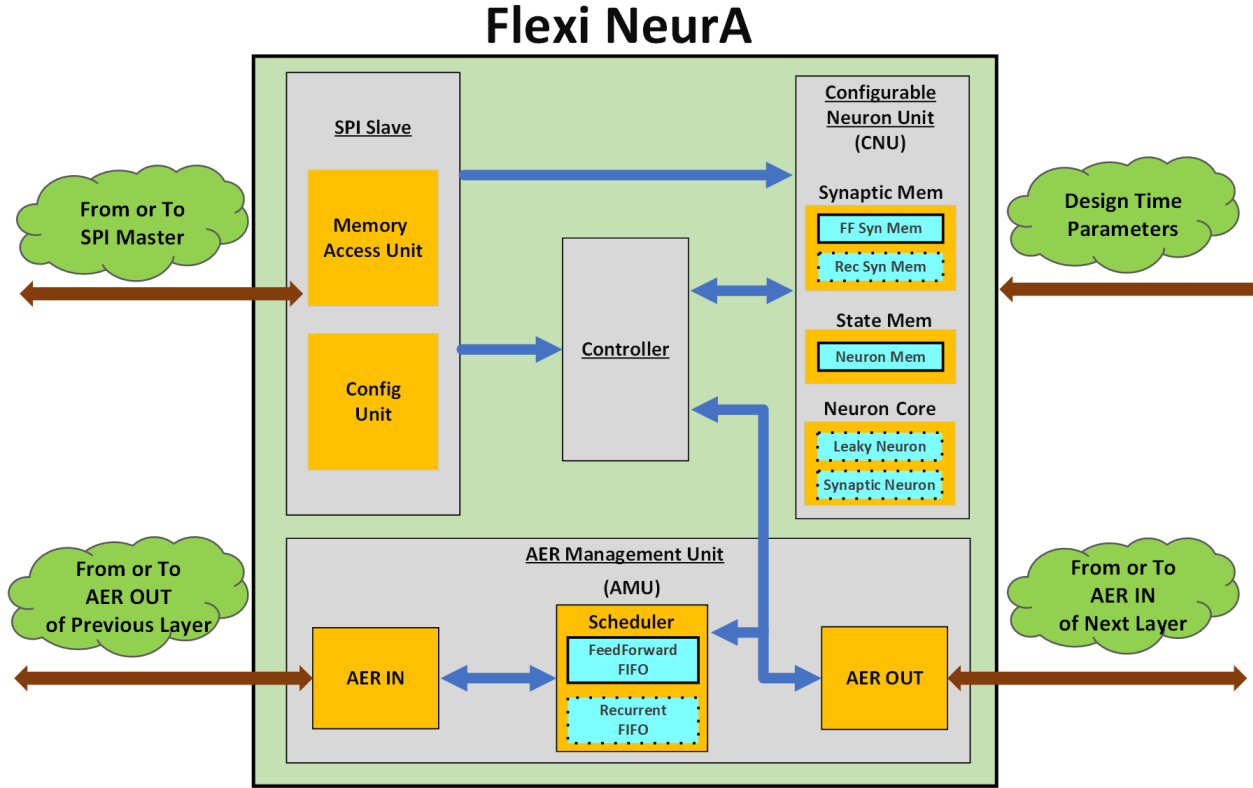


Figure 3: Top-level architecture of the Flexi-NeurA processing core and its main functional units.

Within each layer, incoming ASPL packets sequentially update neurons using the corresponding synaptic weights. In recurrent configurations, ASCL packets are processed similarly. After integration, neurons exceeding the firing threshold emit ASPL packets, while others undergo leakage update.

The network consists of input layer followed by multiple hidden layers and an output layer, with each hidden and output layer mapped to a dedicated Flexi-NeurA core. Inter-core communication occurs exclusively via address-event packets, specially ASCL, EOTS, and EOIN, which are transferred from the AER-OUT port of layer L to the AER-IN port of layer $L+1$. This packet-based pipeline enables layer-by-layer propagation without shared memories or side channels, as illustrated in Fig. 4.

A high-level driver acts as the input layer, SPI master, and output handler. It injects encoded spike streams into the first core, issues EOTS and EOIN packets according to the time step, and collects output events from the final core to determine the predicted class. In addition, the driver programs each core through the SPI interface by loading synaptic weights, initializing neuron states, and configuring parameters such as neuron model, leak coefficients, thresholds, and active neuron count.

Flexi-NeurA exposes key architectural choices as HDL design-time parameters, allowing specialization prior to synthesis. Designers can select neuron models, network topology, and numerical precision to match application-specific accuracy, latency, and resource constraints. Memory dimensions are derived automatically from these parameters, ensuring efficient allocation proportional to network size and precision.

The supported network topologies include feedforward, recurrent All-to-All False, and recurrent All-to-All True. Hardware support is provided for Leaky Integrate-and-Fire and Synaptic neuron models, while the Integrate-and-Fire model is realized by disabling the leak term in the Leaky Integrate-and-Fire implementation.

Designers can specify the bit-width for synaptic weights, membrane potentials, and synaptic currents. Higher precision improves temporal accuracy and stability at the cost of increased area and power, whereas lower precision reduces resource usage. Threshold and reset values are automatically rescaled to match the selected precision, and memory sizes scale with both the number of neurons and the bit-width parameter, ensuring efficient use of on-chip memory.

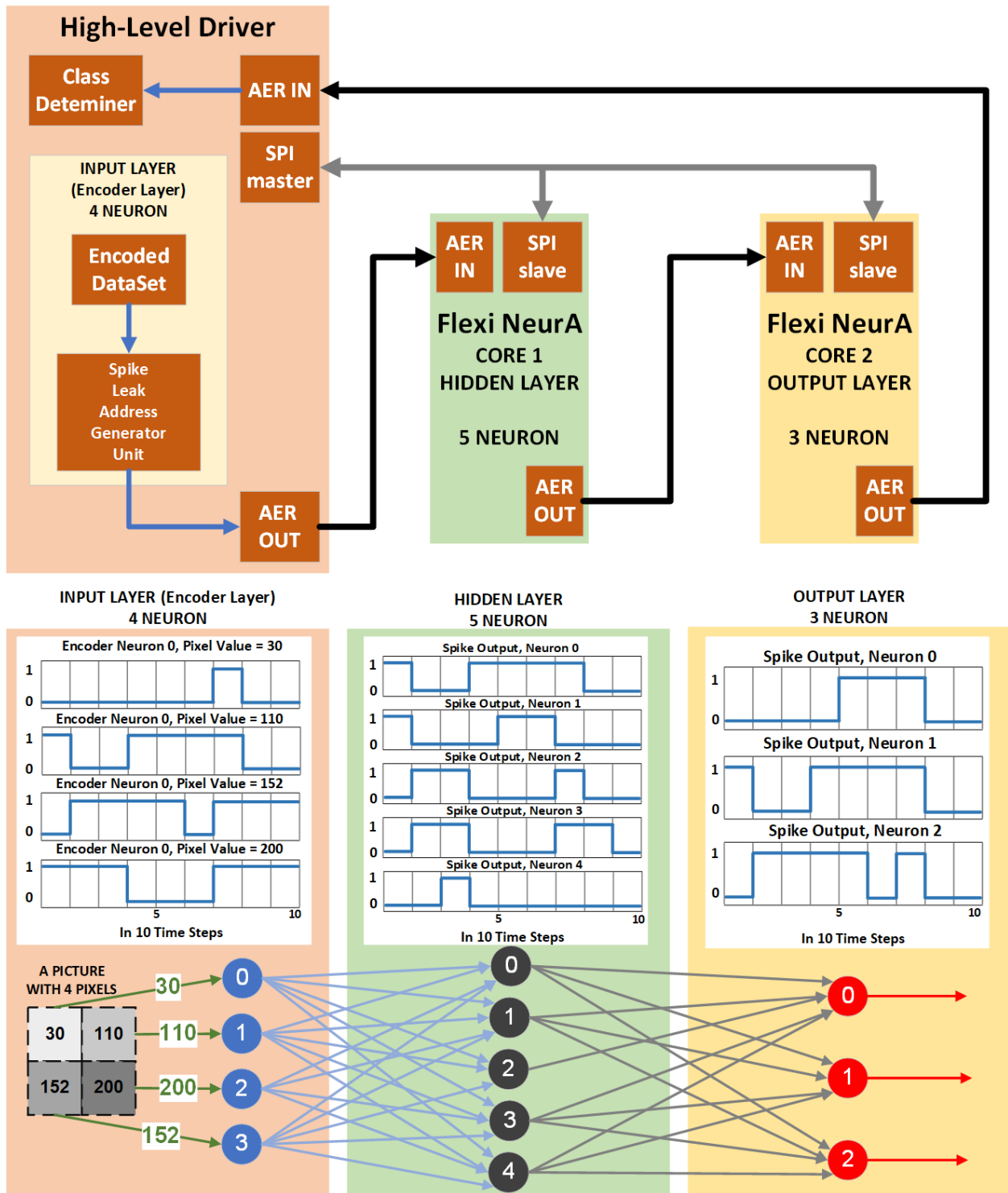


Figure 4: Multi-core system organization showing AER-based inter-layer communication and layer-to-core mapping.

4.1 Hardware Design Components

As shown in Fig. 3, to achieve its flexibility, Flexi-NeurA incorporates several key configurable components, enabling optimized performance tailored to the specific needs of the SNN.

4.1.1 Configurable Neuron Unit (CNU)

The CNU is the core computational module in Flexi-NeurA, responsible for updating all neuron states. It is a highly modular unit composed of dedicated memories for storing parameters and a computational core for executing neuron logic. The entire datapath of the CNU, including its memories and computational units, is designed to be parametric, meaning its structure and bit-precision are configured at design time to match the specific requirements of the application, thereby optimizing hardware resource usage. The CNU comprises three components—Synaptic Memory, Neuron State Memory, and Neuron Core:

a) Synaptic Memory

Memory for weights from the previous layer and a Recurrent Synaptic Memory for weights within the same layer.

The key feature of this memory system is its design-time configurability, which allows both the existence of the recurrent memory and the size of each memory to be determined based on user-defined configuration parameters. Specifically, the recurrent synaptic memory is only instantiated if the network is recurrent and uses the ATA-T topology. Otherwise, it is omitted during synthesis to save resources.

This approach ensures that the memory footprint is optimized, avoiding unnecessary hardware cost. The final memory structure is shaped by the network’s topology and the chosen bit-precision for the weights.

The memory is organized into blocks, with each block containing multiple rows, and each row stores 8 synaptic weights. Memory-space optimization is performed at three levels: (i) Number of Blocks, (ii) Rows per Block, and (iii) Row Width:

1) Number of Blocks: This is determined by the number of spike source neurons (neurons in the previous layer for feed-forward memory, or neurons in the current layer for recurrent memory). This value is rounded up to the nearest power of two for efficient, fixed-bit addressing. For example, a layer with 110 presynaptic neurons would be allocated 128 (2^7) blocks, requiring 7 most significant bits in the address for block selection.

2) Rows per Block: This is based on the number of destination neurons (neurons in the current layer). This number is divided by 8 (since each row holds 8 weights), and the result is rounded up to the nearest power of two. For instance, a layer with 90 spike source neurons (postsynaptic neurons) would require 12 rows, which is rounded up to 16 (2^4) rows, requiring 4 least significant bits in the address for row indexing within each block.

3) Row Width: The width of each memory row in bits is the number of weights per row (8) multiplied by the user-defined bit-precision of the weights (e.g., 4, 6, or 8 bits).

This automated configuration ensures that the memory is precisely scaled to the network’s needs, balancing performance and hardware cost.

b) Neuron State Memory

This memory is a RAM that stores the dynamic state variables for each neuron in the layer. Each neuron is assigned a dedicated row, where the membrane potential (V_m) and synaptic current (I_{syn}) are stored. Like the synaptic memory, this structure is configured at design time; memory-space optimization is performed at two levels: (i) Row Width and (ii) Number of Rows:

1) Row Width: The width of each row corresponds to the total number of bits required to store all state variables for a single neuron. The designer specifies the bit-width for each parameter (e.g., 9 bits for potential, 8 bits for current), and the total (17 bits in this case) is rounded up to the nearest byte boundary (24 bits) for efficient memory access.

2) Number of Rows: The depth of the memory is determined by the number of neurons in the layer, which is also rounded up to the nearest power of two for streamlined addressing.

c) Neuron Core

The Neuron Core is the computational engine of the CNU that executes the logic of the neuron model. It fetches parameters from the Synaptic Memory, Neuron State Memory and Configuration Registers, performs computations, and writes the updated results back to the Neuron State Memory. At design time, the type of neuron model—either LIF, IF, or Synaptic—is selected and synthesized based on user-defined configuration parameters, enabling architectural flexibility. The Neuron Core implements two operations, (i) Integration and (ii) Spike Generation/Leakage:

1) **Integration:** For each ASPL/ASCL event, the controller decodes the spike source, fetches the quantized weight, reads the destination neuron’s state (membrane potential or synaptic current), performs the per-neuron update, and writes the updated state back—only that neuron’s parameters are accessed and modified.

2) **Spike Generation/Leakage:** Upon detecting EOTS/EOIN, the controller activates this phase: neurons are processed sequentially (time-multiplexed); for each neuron, it reads the state, checks the threshold—if exceeded, it registers a spike and applies the configured reset; otherwise, it applies leakage via the Coefficient Generator Unit to the membrane potential (and synaptic current, if used) and writes the updated state back.

4.1.2 Coefficient Generator (CG)

It models leakage in neurons without multipliers, enabling precise and low-cost decay modeling in fixed-point hardware. It employs a five-block shift-and-add network—as shown in Fig. 5—comprising one bypass block and four data blocks, each supporting two right-shift levels: (1,2), (3,4), (5,6), and (7,8) bits. These blocks correspond to the four Selection Units 1–4 in the figure, allowing flexible approximation of any decay factor $k/256$ within the $[0, 1]$ range, where k is an integer between 0 and 255. This enables leakage resolution with $1/256$ granularity and a worst-case rounding error below $1/512$.

The target coefficient is encoded in a 9-bit register `DecayRate[8:0]`, where bit 8 activates the bypass path (Selection Unit 0)—as illustrated at the top of Fig. 5—effectively applying no decay, which is useful for modeling ideal IF model behavior. Bits 7 through 0 enable individual partial shifts across the four blocks. For example, bit 7 selects the shift by 1 ($IN \gg 1$), bit 6 selects shift by 2 ($IN \gg 2$), and so on down to bit 0, which selects shift by 8. Each pair of bits controls one adder block (see the four dashed boxes in Fig. 5), and the outputs are accumulated using a Tree Adder, visible at the right of the figure.

To realize a decay factor of 0.59765625 ($k = 153$), the binary encoding “010011001” is used. This configuration selects the shift paths for $1/2$, $1/16$, $1/32$, and $1/256$, summing their outputs to match the desired value. The selected shift outputs, seen in Fig. 5 as purple paths, are gated and summed, with unused paths effectively zeroed.

Furthermore, the CG architecture supports design-time configurability through the 4-bit parameter `SelectionUnits[3:0]` (as shown in Fig. 5), which specifies whether each of the four data blocks is synthesized. This allows the designer to exclude unnecessary shift blocks from synthesis—such as in simpler neuron models like IF—thereby reducing hardware area and power consumption. Since the CG performs only shift-and-add operations, it inherently maintains symmetry for signed arithmetic, even when certain blocks are omitted.

This architecture thus offers a scalable and efficient solution for implementing continuous-valued decay in event-driven spiking neurons without requiring dedicated multipliers.

4.1.3 Serial Peripheral Interface (SPI)

The SPI module serves as the primary interface for an external master to configure the core and access its internal memories. It has two main functions: writing parameters to the internal configuration registers and performing byte-by-byte read/write operations on the three main memories (Neuron State, Feedforward Synaptic, and Recurrent Synaptic).

a) R/W Memory Operations

All SPI transactions use a fixed 46-cycle frame with two phases: (i) Address Phase (cycles 0–22) and (ii) Data Phase (cycles 23–45), as shown in Fig. 6:

1) **Address Phase (Cycles 0–22):** In the first half of the SPI transaction, a 23-bit command is shifted in on MOSI and, by the end of cycle 22, the full word $a[22:0]$ is latched into the `AddrReg` (Fig. 6). This command packs control and addressing: bit[22] selects the mode (memory access = ‘1’, configuration write = ‘0’), bit[21] is the memory R/W flag (read = ‘0’, write = ‘1’), bits[20:19] choose the target (Neuron State = “00”, Feedforward Synaptic = “01”, Recurrent Synaptic = “10”), and bits[18:0] carry the payload—either the configuration-register index or the row+byte address within the selected memory.

2) **Data Phase (Cycles 23–45):** The second half is for data transfer. In write mode (Fig. 6A), 23 bits of data are received via MOSI. In read mode (Fig. 6B), 8 bits of data are transmitted on the MISO line, starting around cycle 36.

Using the fixed 46-cycle SPI frame, the interface provides access to (i) the Neuron State Memory and to (ii) the Synaptic Memories (Feedforward and Recurrent):

1) **Neuron State Memory access:** This mechanism uses a 23-bit address command: set bit[22] = ‘1’ (memory operation) and bits[20:19] = “00” (select Neuron State). The address payload [18:0] is split as [7:0] = neuron row and [18:8] =

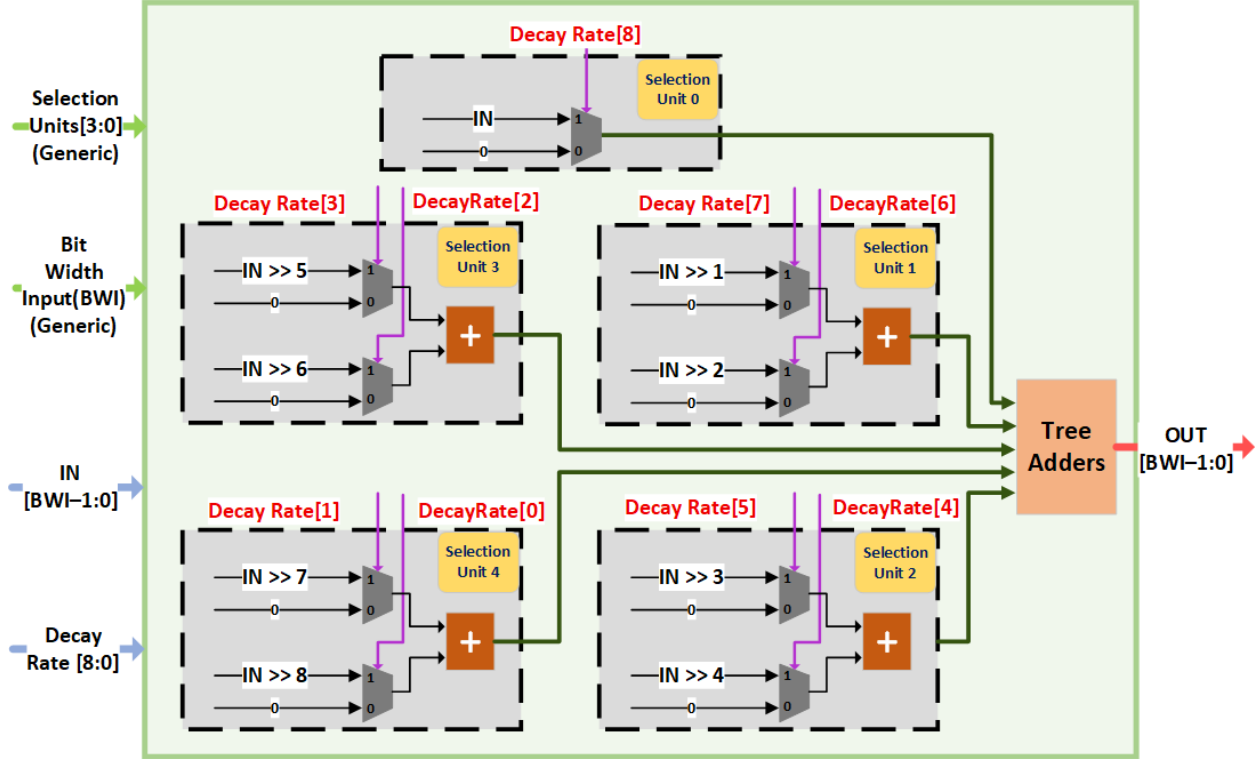


Figure 5: Coefficient Generator (CG) structure based on a shift-and-add network. The 9-bit DecayRate[8:0] configures selectable shifts to approximate any leakage factor in the $[0, 1]$ range with $1/256$ resolution.

byte offset within that row’s state. The read/write flag bit[21] chooses direction, and the 8-bit data is transferred during the second 23-cycle phase—the same format applies for both reads and writes.

2) Synaptic Memory Access: It uses the same 23-bit command but a map tailored to the larger synaptic arrays. Set bit[22] = ‘1’ (memory operation) and choose the target via bits[20:19]— Feedforward = “01”, Recurrent = “10”. Decode the payload [18:0] as [12:0] = row index and [18:13] = byte offset within that row. Data is transformed as 8-bit reads/writes during the second 23-cycle phase, providing uniform, byte-level control of synaptic weights.

b) Configuration Registers

During the configuration, a single master communicates with multiple slave cores in the system. To enable selective communication, each core (slave) is assigned a unique identifier through a design-time parameter defined prior to synthesis. This ID remains fixed for each instance and distinguishes one core from another.

At the beginning of the configuration process, the master writes a value to the SPI core number register in all cores simultaneously. Each core internally compares the received value against its own predefined ID. If the register value matches the core’s ID, that core is flagged as the active target and is subsequently allowed to accept and execute configuration commands.

Design-time parameters define the structural aspects of the accelerator before synthesis—such as neuron models, network topology, and memory dimensions. In contrast, configuration registers are runtime-accessible and dynamically influence computational behavior during execution. The SPI module programs 12 write-only configuration registers that set the core’s operating parameters—covering controller coordination, neuron-core control, and internal SPI state (Fig. 7).

4.1.4 AER Management Unit (AMU)

This unit handles handshake-based reception and transmission of event packets and while preserving their processing order. It buffers and orders packets arriving from the previous layer as well as packets generated locally by the current layer in recurrent modes. The unit comprises three submodules: (i) AER-IN for handshake-based reception, (ii)

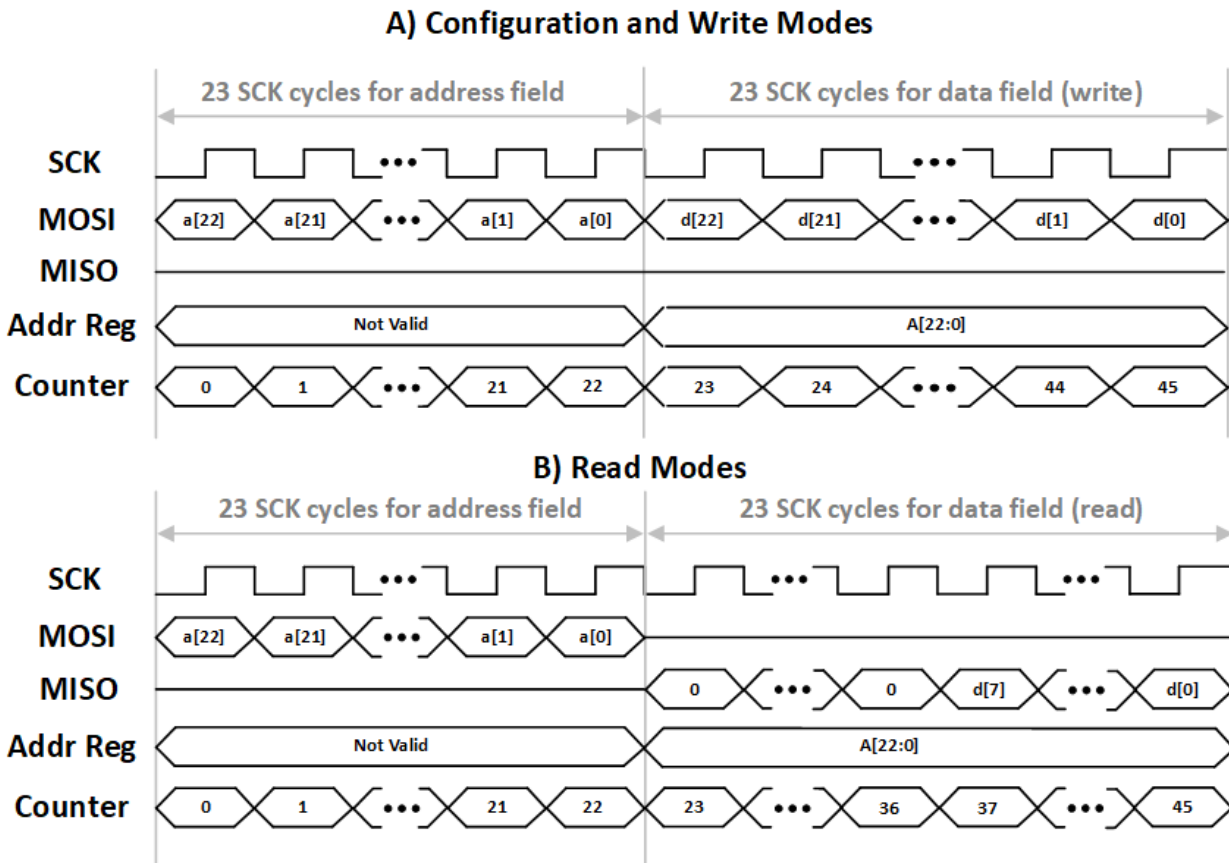


Figure 6: SPI communication timing. (A) Configuration and write operations using 23-bit address and data fields. (B) Read operation with 23-bit address input and 23-bit data output via MISO.

Dest : Controller		Dest : CNU/Neuron Core		Dest : As a Internal Reg in SPI Slave	
Spi core number	SPI ACTIVITY En	SPI Neuron Number	SPI FEEDFORWARD RECURRENT		
SPI NEURON MODEL LEAKY/SYNAPTIC	SPI TIME STEP	SPI ALL TO ALL	SPI ALL TO ALL FALSE WEIGHT		
SPI THRESHOLD	SPI RESET MECHANISM	SPI BETA RATE	SPI ALPHA RATE		

Figure 7: Configuration registers and their functional destinations within the Flexi-NeurA core.

AER-OUT for handshake-based transmission, and (iii) a scheduler for queueing and ordering inbound, outbound, and internal events:

1,2) AER-IN and AER-OUT: AER-IN handshakes with the previous layer to receive ASPL, EOTS, and EOIN packets and, when the feedforward scheduler has space, forwards them to the scheduling queue. AER-OUT handshakes with the next layer to transmit locally generated ASPL, EOTS, and EOIN packets.

3) Scheduler: The scheduler comprises two FIFO-based queues. The feedforward scheduler accepts external event packets (ASPL, EOTS, EOIN) from AER-IN and forwards them to the controller in arrival order. The recurrent scheduler buffers ASCL packets generated within the same layer for reuse in recurrent computation; it is instantiated only when recurrence is enabled at design time, and otherwise omitted to conserve hardware resources.

4.1.5 Controller

The controller is the core’s central operational unit, managing all processes through four main phases—(i) configuration, (ii) spike integration, (iii) leakage/spike generation, and (iv) packet transmission:

a) Configuration Phase

During the configuration phase (highest priority), the core is initialized via SPI: a controller state machine (Fig. 8) decodes each SPI command and selects the proper memory path, then issues targeted reads/writes to the feedforward synaptic, recurrent synaptic, and neuron-state memories. Based on the opcode, it enters one of six microstates (e.g., R/W NEUR, R/W FF SYN, R/W REC SYN) to perform a single-cycle memory access for deterministic loading of weights and neuron parameters. After each access, the controller transitions to WAIT_SPI to synchronize with the slower SPI bus before proceeding, ensuring transfer completion and avoiding timing-related data corruption.

b) Spike Integration Phase

During this phase, the controller processes incoming spike event packets (ASPL and ASCL) that are queued in the scheduler:

1) Feedforward Integration: The controller services ASPL packets dequeued from the feedforward scheduler. For each packet, it enters FF-Integ (Fig. 9), decodes the source address, and—using a time-multiplexed compute unit—sweeps the current layer neuron-by-neuron: for each neuron it fetches the corresponding synaptic weight and state (V_m/I_{syn}), accumulates the contribution, and writes back the updated state. After all neurons are updated, it advances to the next ASPL in the feedforward FIFO.

2) Recurrent Integration: Upon receiving EOTS/EOIN, the controller enters REC-Integ—either ATA-T (all-to-all true) or ATA-F (all-to-all false)—and services ASCL packets from the recurrent scheduler. In ATA-T, for each ASCL the time-multiplexed compute unit sweeps all neurons: it reads the recurrent weight and current neuron state, accumulates the contribution to V_m/I_{syn} , and writes back to the Neuron State Memory. In ATA_F, only the source neuron is updated using its self-recurrent weight. Processing proceeds packet-by-packet and neuron-by-neuron until the ASCL queue is drained.

c) Leakage/Spike Generation

After all ASPL/ASCL effects are integrated for a step, the controller enters Leak/Spk (Fig. 9) and evaluates neurons sequentially with the time-multiplexed unit. For each neuron: if its membrane potential reaches or exceeds its threshold, a spike is generated—an ASPL packet is sent to the next layer and, if the network is recurrent, an ASCL packet is also enqueued locally—then the neuron is reset. Otherwise, leakage is applied to the membrane potential (and to the synaptic current, if modeled). At the final step of a sample (EOIN), a lazy reset writes zeros directly to the neuron’s state instead of the computed value, avoiding global clears and preparing the core for the next sample.

d) Packet Transmission

After generating a spike, the controller enters the Wait-Trans state (as shown in Fig. 9) to synchronize with the next layer. It holds the packet until the feedforward queue of the next layer is full, ensuring the lossless transfer of data and naturally handling backpressure. Afterward, the controller sends a control packet: it sends an EOTS (End of Time Step) packet if additional time steps are needed, or an EOIN (End of Input) packet if it is the final step.

5 Exploration

Design-space exploration (DSE) is the systematic process of evaluating many design configurations under user-specified constraints and selecting the lowest-cost option. To automate this, we use Flex-plorer as an end-to-end flow in which a GUI collects all required inputs; the network is trained to obtain weights and leak parameters; the Explorer then

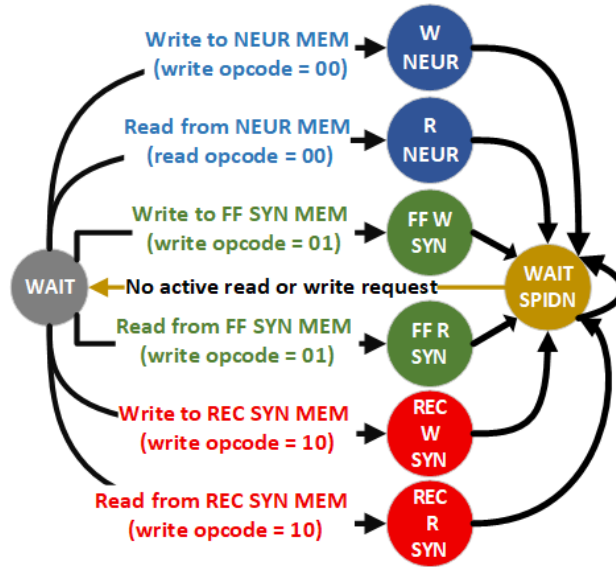


Figure 8: Controller state machine for handling read/write operations across neuron, feedforward synapse, and recurrent synapse memories, including SPI wait synchronization.

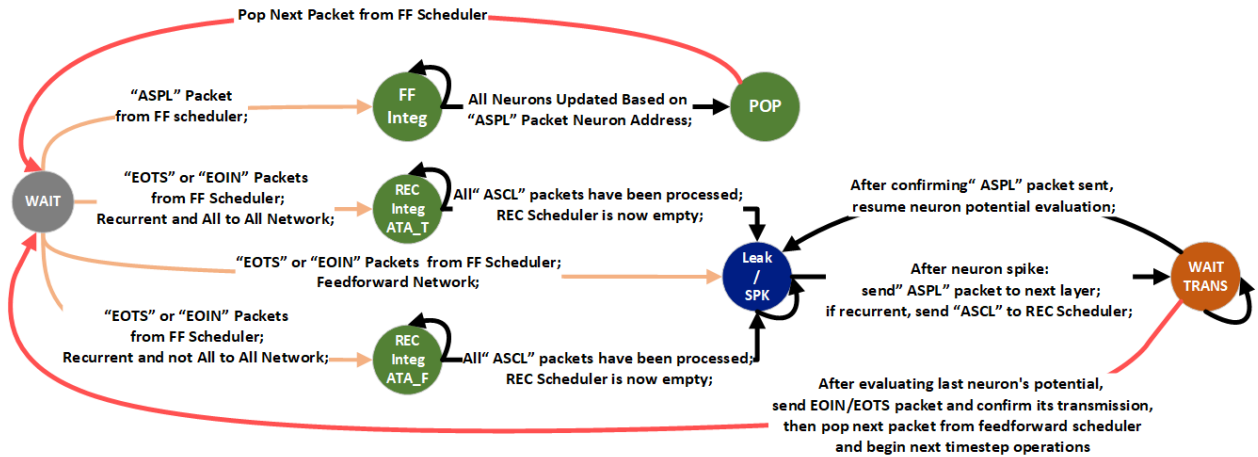


Figure 9: State machine for the controller's Spike Integration and Leakage & Spike Generation phases. Incoming spike packets from feedforward or recurrent paths trigger per-neuron updates, followed by potential evaluation, spike emission, and control signaling (EOTS/EOIN).

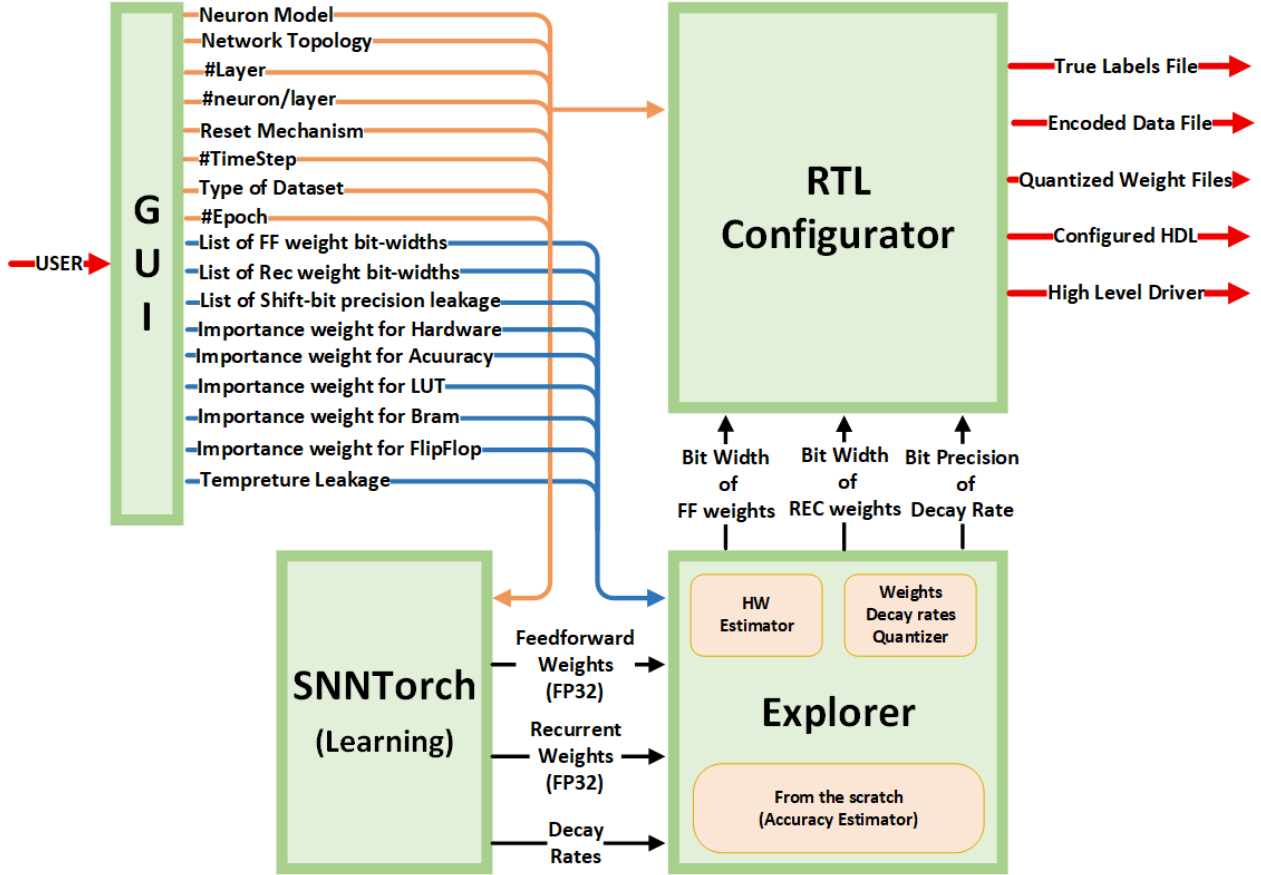


Figure 10: Overview of the Flex-plorer framework for design-space exploration and hardware generation.

searches within user-defined priorities and bounds to pick the best configuration; and finally, the RTL Configurator parameterizes reusable RTL templates for the chosen architecture and emits a ready-to-implement package—configured RTL, quantized weight files, encoded datasets/labels, and a driver (Fig. 10).

First, Flexi-NeurA creates a large design space, offering numerous configuration possibilities. To narrow down this space, the user specifies parameters through the GUI, such as network topology, neuron model, layer count, number of neurons, reset policies, and bit-precision bounds for feed-forward and recurrent weights, as well as leak precision. This process limits the search space to the desired boundaries for bit-widths of weights and leak precision (managed by the CG module).

After the GUI collects all required inputs, the Learning stage trains the user-specified network based on these settings, using SNN-Torch. After training, the network’s weights and layer-wise leak parameters are extracted and passed to the Explorer. With the architecture fixed, DSE focuses on three precision knobs: feedforward weight bit-width, recurrent weight bit-width (if recurrence is enabled), and the leakage bit-precision used by the Coefficient Generator, yielding a finite set of candidates. We perform DSE using simulated annealing: each candidate is evaluated in terms of task accuracy and hardware cost, and the lowest-cost configuration that satisfies the user’s constraints is selected.

Finally, the RTL Configurator parameterizes reusable RTL templates according to the chosen architecture: per-layer topology (FF / ATA-F / ATA-T), neuron model (IF / LIF / Synaptic), bit-widths for weights, membrane potentials, and synaptic currents, and the time-multiplexing schedule. It also generates a matching driver and converts the chosen dataset into an event-encoded input format, delivering a ready-to-run package for hardware implementation or simulation.

We use simulated annealing to explore hardware configurations with the help of two functions: an accuracy evaluator that is functionally identical to the hardware (bit-exact arithmetic and the same update/control order), and a hardware-cost estimator.

Due to Flexi-NeurA’s time-multiplexed, neuron-by-neuron execution, we can mirror the hardware’s exact update order and fixed-point arithmetic, resulting in a simulator that is functionally identical to the deployed hardware.

We use a hardware usage estimator to predict the number of flip-flops, block RAMs, and LUTs for each configuration. This estimator makes its predictions based on factors such as the number of neurons in the previous and current layers, the number of layers, network type, and neuron type. It estimates values that are close to the actual resource usage. This process is performed separately for flip-flops, block RAMs, and LUTs as follows:

LUTs and flip-flops: At the core level, we profile three network topologies and two neuron types (the IF neuron is realized using the LIF implementation). To keep the analysis focused, we hold low-sensitivity hardware parameters fixed and vary only the bit-widths of the feedforward and recurrent weights. For each resulting in-core configuration, we run synthesis and record the LUT and flip-flop counts. This produces a clean data table that covers all topology–neuron combinations across a range of weight precisions.

Using this table, we then fit two lightweight regression models per core—one for LUTs and one for flip-flops—whose inputs are the bit-widths of the feedforward and recurrent weights. Trained on post-synthesis measurements, these models accurately predict resource usage closely while being fast to evaluate.

BRAM: From empirical FPGA synthesis and BRAM mapping, we built a parametric model linking BRAM usage to network topology, neuron model, bit-widths, and neuron count—producing estimates that closely match post-synthesis allocations.

Finally, layer-level usage is obtained by summing the predictions of the cores that implement that layer. This straightforward procedure gives accurate, transparent estimates of LUT and flip-flop demand for any target configuration and supports efficient design-space exploration.

Having defined the hardware-cost and accuracy-cost functions, we compute the total cost of each configuration as their weighted sum. Two user-set weights, C_H and C_A (summing to 1 as shown in Eq. 7), control the relative influence of hardware versus accuracy. The accuracy term (Eq. 4) is obtained by first estimating accuracy and then mapping it to an accuracy cost, while the hardware term (Eq. 5) combines normalized LUT, flip-flop, and BRAM usage using weights C_{LUT} , C_{FF} , and C_{BRAM} (also summing to 1 as shown in Eq. 7) to reflect user priorities. Adding these two terms yields a single tunable total cost (Eq. 6) per configuration, enabling efficient, preference-aware design-space exploration. To search this space, we choose simulated annealing (Listing 1): inspired by metallurgical annealing, it mitigates entrapment in local optima, handles discrete and irregular design-spaces, and provides a clean exploration–exploitation trade-off via a temperature schedule.

$$HwCost = C_H(C_{LUT}LUT_n + C_{FF}FF_n + C_{BRAM}BRAM_n) \quad (4)$$

$$AccCost = C_A(1 - hardware_aware_accuracy) \quad (5)$$

$$TotalCost = HwCost + AccCost \quad (6)$$

$$\text{subject to } \begin{cases} C_H + C_A = 1 \\ C_{LUT} + C_{FF} + C_{BRAM} = 1 \end{cases} \quad (7)$$

We choose simulated annealing (Listing 1): inspired by metallurgical annealing, it mitigates entrapment in local optima, handles discrete and irregular design spaces, and provides a clean exploration–exploitation trade-off via a temperature schedule. The user specifies the network architecture and search bounds (feedforward bit-width, recurrent bit-width, leak coefficient) and sets five importance weights governing the accuracy term and the three hardware resources (LUT, flip-flop, BRAM) (lines 1-7). All candidate configurations consistent with these bounds are then enumerated, and—prior to annealing—we pre-compute and cache normalized LUT/flip-flop/BRAM usage and aggregate them into a hardware cost for every configuration (lines 8-13). The annealing phase starts from a random configuration and an initial temperature (lines 14-17); at each temperature only a fraction of the space (e.g., one-half or one-third) is probed by proposing neighbors that change exactly one knob (feedforward bits, recurrent bits, or leak) (lines 21-24). Accuracy is retrieved from a cache when available (otherwise computed once and stored), combined with the cached hardware cost to form a total cost, and evaluated under the annealing acceptance rule: strictly better moves are accepted, while worse moves may be accepted with a probability that decreases as the temperature cools. Whenever a new best cost is observed, the incumbent best is updated. The temperature is gradually reduced until a minimum threshold is reached, at which point the configuration with the lowest total cost is returned (lines 25-32).

Listing 1: Simulated annealing procedure used for precision-aware design-space exploration

```

1   # user selects architecture and weights
2   Arch <- get_arch()
3   Ca,Ch <- get_w_acc_hw()           # ca+ch=1
4   w_lut,w_ff,w_bram <- get_w_hw()   # sum=1
5
6   # exploration ranges and eval divisor (e.g., k=2 for half, k=3 for third)
7   ff_range, rec_range, leak_bit_acc <- get_ranges()
8   k <- get_eval_divisor()           # User-defined space exploration fraction
9
10  # enumerate candidates and precompute hardware cost
11  cfgs <- enum_cfgs(arch, ff_range, rec_range, leak_bit_acc)
12
13  # Precompute hardware cost for all configurations
14  for cfg in cfgs:
15    hw_cost[cfg] <- hw_cost_Estimator(cfg)
16
17  # simulated annealing (cost formulas omitted inside the loop)
18  Simulated-Annealing():
19    cur_cfg <- random_cfg(cfgs)       # Select a random configuration
20    best <- cur_cfg                   # Set current as best
21    T <- T_start                      # User-defined initial temperature
22
23    # Total cost for random configuration
24    cur_cost <- total_cost(cur_cfg, hw_cost[cur_cfg], acc_cost(cur_cfg))
25    best_cost <- cur_cost
26
27    while T > T_min:
28      n <- max(cfgs/k)                # how many cfg process around a configuration
29
30      for i to n:
31        nbr <- neighbor(cur_cfg, cfgs) # select a neighbor
32
33        # Total cost for neighbor of selected configuration
34        nbr_cost <- total_cost(nbr, hw_cost[nbr], acc_cost(nbr))
35
36        # Calculate difference between neighbor and current cost
37        Δ <- nbr_cost - cur_cost
38
39        # take better moves, otherwise accept worse with probability
40        if (Δ <= 0) or (rand() < exp(-Δ/T)):
41          cur_cfg, cur_cost <- nbr, nbr_cost
42          if (cur_cost < best_cost): # Update best configuration if improved
43            best, best_cost <- cur_cfg, cur_cost
44
45    T <- α*T                          # lowering the temperature

```

6 Results and Comparisons

We evaluate Flexi-NeurA end-to-end on three representative benchmarks: MNIST, Spiking Heidelberg Digits (SHD), and DVS Gesture, using the Flex-plorer framework. As dictated by the core architecture (Fig. 3) and the per-layer mapping strategy (Fig. 4), each Flexi-NeurA processing core supports up to 256 neurons. Accordingly, all datasets are preprocessed to satisfy this per-layer constraint.

For MNIST, grayscale images of handwritten digits (28×28) are downscaled to at most 16×16 and normalized. Pixel intensities are converted into spike trains using rate encoding over a fixed inference window, yielding no more than 256 input channels. The SHD dataset consists of event-based auditory spike streams from 700 cochlear channels representing spoken digits across 20 classes. To meet hardware constraints, channel reduction by a factor of $k > 2$ is applied such that $700/k < 256$, followed by mapping the incoming spike streams onto discrete time steps that are

Table 1: Trained network configurations and classification accuracy across datasets, neuron models, and topologies.

#	Neuron	Network	Dataset	#Time Step	Accuracy
1	LIF	FF	MNIST	100	98.05%
2	Synaptic	FF	DVS	70	71.11%
3	LIF	ATA-F	DVS	60	82.20%
4	IF	FF	MNIST	80	97.10%
5	Synaptic	FF	SHD	80	67.56%
6	Synaptic	FF	MNIST	60	97.65%
7	IF	ATA-T	MNIST	50	97.20%
8	IF	ATA-T	SHD	70	67.15%
9	LIF	FF	SHD	110	70.89%
10	LIF	ATA-F	MNIST	50	96.20%
11	LIF	ATA-F	SHD	60	64.71%
12	LIF	ATA-T	DVS	80	85.79%
13	LIF	ATA-T	MNIST	50	96.51%
14	Synaptic	ATA-T	SHD	120	76.69%
15	LIF	ATA-T	SHD	80	75.56%
16	IF	ATA-F	DVS	70	83.33%
17	IF	ATA-F	MNIST	40	97.07%
18	LIF	FF	DVS	60	84.56%
19	IF	FF	DVS	60	85.23%
20	IF	FF	SHD	50	66.08%

synchronized with the accelerator’s internal update cycle. No artificial spike encoding is required, as SHD is inherently spike-based. The DVS Gesture dataset comprises of 11 hand-gesture classes captured by a 128×128 event camera. A lightweight convolutional pre-processing stage extracts and compresses spatial features to fewer than 256 channels, after which thresholding is applied to generate binary spike events used for inference.

Each network layer is mapped to a dedicated processing core, and inter-layer communication is realized exclusively through address-event packets, as illustrated in Fig. 4. While event streams are naturally accommodated by the event-driven execution model, the architecture also remains correct under high-traffic and dense spiking conditions. Inter-core event transfer is handled through a handshake-based protocol that provides backpressure and buffering, guaranteeing lossless communication even when event rates are high. As a result, all spike events are processed deterministically regardless of input sparsity.

All networks are trained offline using backpropagation-through-time with surrogate gradients implemented in SNN-Torch. Following training, floating-point synaptic weights and leak coefficients (α, β) are extracted prior to quantization. A representative subset of trained configurations and their corresponding classification accuracies is reported in Table 1, highlighting the impact of neuron model, network topology, and inference time steps across datasets.

Table 2 compares Flexi-NeurA with recent FPGA-based accelerators on the MNIST benchmark. The compared designs can be broadly divided into two categories: hybrid SCNN accelerators, which incorporate convolutional front-ends, and pure SNN accelerators composed of fully connected IF or LIF layers. Hybrid SCNN designs generally report higher classification accuracy due to their larger and more complex network structures. In contrast, pure SNN accelerators prioritize hardware efficiency. Within this class, Flexi-NeurA achieves the highest reported accuracy, reaching 97.23% on MNIST. This result highlights the effectiveness of Flexi-NeurA in balancing accuracy and efficiency within fully spiking network architectures.

On a Xilinx Zynq-7000 XC7Z020 FPGA, the selected MNIST configuration implements a three-layer fully connected SNN with LIF neurons (256-128-10) and 6-bit quantized weights, mapped to two processing cores. Core 1 hosts the hidden layer, while Core 2 implements the output layer. Post-synthesis results obtained using Vivado show a combined footprint of 1,623 logic cells, 934 LUTs, 689 flip-flops, and 7 BRAM blocks, corresponding to approximately 4%, 3%, 1%, and 5% of device resources, respectively. Total power consumption is measured at 111 mW, dominated by static power. Compared to the state of the art shown in Table 2, Flexi-NeurA reports the lowest power consumption and logic utilization, demonstrating the effectiveness of time-multiplexed execution for edge-oriented SNN acceleration.

Flexi-NeurA classifies a single MNIST image in 1.1ms. Despite limited parallelism, latency remains competitive due to the event-driven execution model, which eliminates idle computation and unnecessary memory accesses. The 60 MHz clock frequency, the 100-cycle controller loop, and per-neuron sequential updates determine the overall delay, yet the

Table 2: Comparison of Flexi-NeurA with recent FPGA-based accelerators on the MNIST benchmark.

Design	Liu et al. [29]	Navarez et al. [34]	Li et al. [33]	Gerlinghoff et al. [32]	Panchapakesan et al. [27]	Khodamoradi et al. [30]
Year	2023	2021	2023	2022	2021	2021
f_{clk} [MHz]	100	200	300	200	200	N/R
Neuron bw	8	8	12	N/R	4	N/R
Weights bw	8	8	8	3	4	N/R
Update	Clock	Clock	Clock	Clock	Event	Event
Model	IF	Spike-by-Spike (SbS)	LIF	LIF	IF	LIF
FPGA	XAZ7020	XC7Z020	XCZU3EG	CXVU13P	XCZU9EG	XAZ7020
Avail BRAM	140	140	216	2,688	912	140
Used BRAM	N/R	16	50	N/R	N/R	40.5
Avail DSP	220	220	360	12,288	2,520	220
Used DSP	0	46	288	0	N/R	11
Avail logic cell	159,600	159,600	211,680	3,088,800	822,240	159,600
Used logic cell	27,551	23,704	15,000	51,000	N/R	39,368
Architecture	28X28-32c3-p2-32c3-p2-256-10	28X28X2-32C3-P2-64C5-P2-1024-10	28X28-16C3-64C3-P2-128C3-P2-256C3-256C3-10	28X28-32c3-p2-32c3-p2-256-10	28X28-32c3-p2-32c3-p2-256-10	28X28-16C7-24C7-32C7-10
#syn	8,960	75,776	2,560	25,320	10,752	320
#time step	N/R	1000	4	4	7-10	N/R
T_{lat}/img [ms]	0.27	1.57	0.49	0.29	0.08	N/R
Power [W]	0.28	0.22	2.55	3.40	N/R	N/R
E/img [mJ]	0.076	0.37	1.25	0.986	N/R	N/R
E/syn [nJ]	8.48	4.88	488	38.90	N/R	N/R
Accuracy	99.00%	98.84%	98.12%	99.10%	99.30%	98.50%

Design	Han et al. [24]	Gupta et al. [28]	Li et al. [25]	Garpenga et al. [31]	SPIKER+ [10]	Flexi-NeurA (this work)
Year	2020	2020	2021	2022	2024	2026
f_{clk} [MHz]	200	100	100	100	100	60
Neuron bw	16	24	16	16	6	8
Weights bw	16	24	16	16	4	6
Update	Event	Event	Hybrid	Clock	Clock	Event
Model	LIF	LIF	LIF	LIF	LIF	LIF
FPGA	XC7Z045	XC6VLX240T	XC7VX485	XC7Z020	XC7Z020	XC7Z020
Avail BRAM	545	416	2,060	140	140	140
Used BRAM	40.5	162	N/R	45	18	7
Avail DSP	900	768	2,800	200	220	220
Used DSP	0	64	N/R	0	0	0
Avail logic cell	655,800	452,160	485,760	159,600	159,600	159,600
Used logic cell	12,690	79,468	N/R	55,998	7,612	1,623
Architecture	784-1024-1024-10	784-16	784-200-100-10	784-400	784-128-10	256-128-10
#syn	1,861,632	12,544	177,800	313,600	101,632	34,048
#time step	N/R	N/R	N/R	3500	100	100
T_{lat}/img [ms]	6.21	0.5	3.15	0.22	0.78	1.1
Power [W]	0.477	N/R	1.6	59.09	0.18	0.11
E/img [mJ]	2.96	N/R	5.04	13	0.14	0.12
E/syn [nJ]	1.59	N/R	28	41	1.37	3.5
Accuracy	97.06%	N/R	92.93%	73.96%	93.85%	97.23%

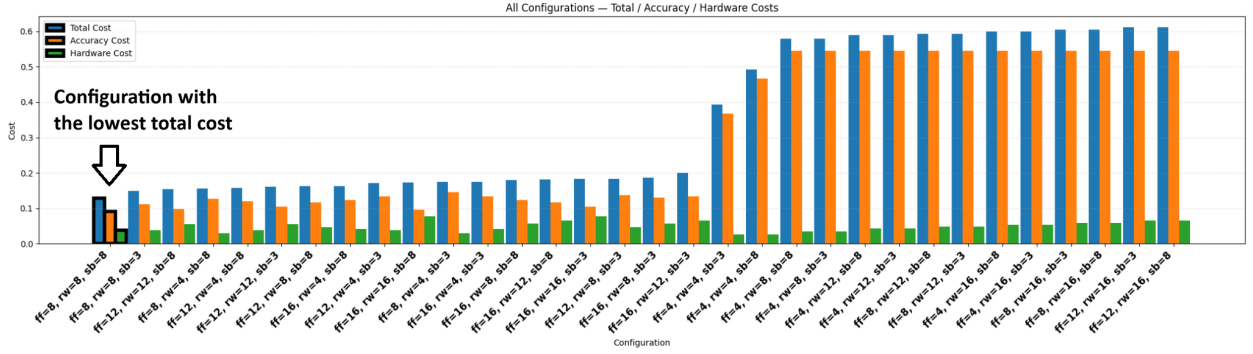


Figure 11: Design-space exploration results illustrating the impact of precision choices on hardware cost and accuracy. DSE setup and outcome for DVS: user specifies a LIF network with ATA-F topology and layers [256, 200, 11]; exploration ranges are defined feedforward weight bit-widths {4, 8, 12, 16}, recurrent weight bit-widths {4, 8, 12, 16}, and for leak precision {3, 8}. Cost weights: HW=0.500, ACC=0.500; resource weights: LUT=0.330, BRAM=0.340, FF=0.330. Chosen configuration: FF-w=8, Rec-w=8, leak bit-acc=8.

architecture avoids the typical latency penalties associated with time-multiplexed designs while maintaining low power and area.

A key scalability property of Flexi-NeurA is that increasing layer width primarily affects BRAM usage, while logic utilization remains nearly constant. Since all neurons within a layer share a single time-multiplexed datapath, the compute logic does not scale with network size. Instead, only synaptic weights and per-neuron state storage grow, resulting in deeper memories rather than wider datapaths. This decoupling enables scalable network expansion with minimal additional logic cost.

The design-space exploration process is dominated by bit-accurate accuracy evaluation in software, which can become a bottleneck when exploring large configuration spaces. To mitigate this, Flex-plorer JIT-compiled the critical evaluation kernels using Numba [26], significantly accelerating execution and enabling practical exploration of extensive precision combinations.

As a concrete example of the design-space exploration process, Fig. 11 illustrates a set of candidate hardware configurations evaluated for an ATA-F network, sorted from left to right by increasing total cost as defined in Section V. Each column represents one explored configuration, characterized by three precision parameters along the horizontal

axis: the bit-width of feedforward synaptic weights, the bit-width of recurrent weights, and the bit-precision of the decay parameters. This visualization highlights how different precision combinations explored by Flex-plorer translate into distinct hardware costs.

For the evaluated ATA-F configuration, feedforward synaptic weights are stored in BRAM, whereas recurrent weights are fixed per layer and therefore implemented as configuration registers rather than memory arrays. As a result, BRAM usage is primarily driven by the number of neurons, the number of layers, and the feedforward weight bit-width. In contrast, LUT and flip-flop utilization is largely determined by datapath width. When recurrent weight precision approaches or exceeds feedforward precision, wider operands propagate through arithmetic and storage units, increasing LUT and flip-flop cost. From an accuracy perspective, maintaining feedforward precision equal to or higher than recurrent precision generally preserves accuracy while minimizing hardware cost. Conversely, configurations in which recurrent precision exceeds feedforward precision often exhibit sharp accuracy degradation due to quantization imbalance.

7 Conclusion

This work introduces a hardware-software platform for SNN acceleration, with Flexi-NeurA at its core. It is a design-time configurable processing core, allowing the selection of neuron models, network topology, reset policy, bit-widths for weights, and synapse counts, ensuring efficient hardware instantiation. Flexi-NeurA leverages event-driven and time-multiplexed execution, achieving high efficiency with low power consumption, while supporting multi-core processing. With 97.23% accuracy on the MNIST, Flexi-NeurA uses only the necessary hardware resources. Flex-plorer, an end-to-end DSE tool, automates configuration by exploring precision trade-offs and generating configured RTL, high-level driver, and encoded dataset inputs. Together, Flexi-NeurA and Flex-plorer enable scalable and efficient SNN implementations for edge-AI applications.

Data Availability

To encourage research in this field, Flex-plorer and Flexi-NeurA are available at <https://github.com/Mohammadfarahani98>.

References

- [1] R. Singh and S. S. Gill, "Edge AI: A Survey," *Internet of Things and Cyber-Physical Systems*, vol. 3, pp. 71-92, 2023.
- [2] Z. Zhou, X. Chen, E. Li, L. Zeng, K. Luo and J. Zhang, "Edge Intelligence: Paving the Last Mile of Artificial Intelligence With Edge Computing," *Proceedings of the IEEE*, vol. 107, no. 8, pp. 1738-1762, 2019.
- [3] E. Li, L. Zeng, Z. Zhou and X. Chen, "Edge AI: On-Demand Accelerating Deep Neural Network Inference via Edge Computing," *IEEE Transactions on Wireless Communications*, vol. 19, pp. 447-457, 2020.
- [4] W. Maass, "Networks of Spiking Neurons: The Third Generation of Neural Network Models," *Neural Networks*, vol. 10, no. 9, pp. 1659-1671, 1997.
- [5] M. Bouvier, A. Valentian, T. Mesquida, F. Rummens, M. Reyboz, E. Vianello and E. Beigné, "Spiking Neural Networks Hardware Implementations and Challenges: A Survey," *ACM Journal on Emerging Technologies in Computing Systems (JETC)*, vol. 15, no. 2, pp. 1-35, 2019.
- [6] K. Roy, A. Jaiswal and P. Panda, "Towards Spike-Based Machine Intelligence with Neuromorphic Computing," *Nature*, vol. 575, no. 7784, pp. 607-617, 2019.
- [7] S. Liu, J. Wang, J. Zhou, S. Hu, Q. Yu, T. Chen and Y. Liu, "An Area- and Energy-Efficient Spiking Neural Network With Spike-Time-Dependent Plasticity Realized With SRAM Processing-in-Memory Macro and On-Chip Unsupervised Learning," *IEEE Transactions on Biomedical Circuits and Systems*, vol. 17, no. 1, pp. 92-104, February 2023.
- [8] H. Liu, Y. Chen, Z. Zeng, M. Zhang and H. Qu, "A Low Power and Low Latency FPGA-Based Spiking Neural Network Accelerator," in *Conference Name: IEEE International Conference on Circuits and Systems (ISCAS)*, 2023.
- [9] G. Indiveri and S.-C. Liu, "Memory and Information Processing in Neuromorphic Systems," *Proceedings of the IEEE*, vol. 103, no. 8, pp. 1379-1397, 2015.

- [10] A. Carpegna, A. Savino and S. D. Carlo, "Spiker+: A Framework for the Generation of Efficient Spiking Neural Networks FPGA Accelerators for Inference at the Edge," *IEEE Transactions on Emerging Topics in Computing*, pp. 1-15, 2024.
- [11] C. Frenkel, M. Lefebvre, J.-D. Legat and D. Bol, "A 0.086-mm² 12.7-pJ/SOP 64k-Synapse 256-Neuron Online-Learning Digital Spiking Neuromorphic Processor in 28-nm CMOS," *IEEE Transactions on Biomedical Circuits and Systems*, vol. 13, 2019.
- [12] C. Frenkel and G. Indiveri, "ReckOn: A 28-nm Sub-mm² Task-Agnostic Spiking Recurrent Neural Network Processor Enabling On-Chip Learning over Second-Long Timescales," in *2022 IEEE International Solid-State Circuits Conference (ISSCC)*, 2022.
- [13] C. Frenkel, J.-D. Legat and D. Bol, "MorphIC: A 65-nm 738k-Synapse/mm² Quad-Core Binary-Weight Digital Neuromorphic Processor with Stochastic Spike-Driven Online Learning," *IEEE Transactions on Biomedical Circuits and Systems*, pp. 1-11, 2019.
- [14] M. Davies, N. Srinivasa, T.-H. Lin, G. N. Chinya, Y. Cao, S. H. Choday, G. D. Dimou, P. Joshi, N. Imam, S. Jain, Y. Liao, C.-K. Lin, A. Lines, R. Liu, D. Mathaikutty, S. McCoy and A. Paul, "A Neuromorphic Manycore Processor with On-Chip Learning," *IEEE Micro*, pp. 82-99, September 2018.
- [15] D. Padovano, A. Carpegna, A. Savino and S. D. Carlo, "SpikeExplorer: Hardware-Oriented Design Space Exploration for Spiking Neural Networks on FPGA," *Electronics*, vol. 13, no. 9, May 2024.
- [16] N. Jannesar, K. Akbarzadeh-Sherbaf, S. Safari and A.-H. Vahabie, "SSTE: Syllable-Specific Temporal Encoding to FORCE-learn audio sequences with an associative memory approach," *Neural Networks*, vol. 177, 2024.
- [17] J. K. Eshraghian, M. Ward, E. O. Neftci, X. Wang, G. Lenz, G. Dwivedi, M. Bennamoun, D. S. Jeong and W. D. Lu, "Training Spiking Neural Networks Using Lessons From Deep Learning," *Proceedings of the IEEE*, vol. 111, no. 9, pp. 1016-1045, 2023.
- [18] A. L. Hodgkin and A. F. Huxley, "A Quantitative Description of Membrane Current and Its Application to Conduction and Excitation in Nerve," *J. Physiol*, vol. 117, no. 1, pp. 500-544, 1952.
- [19] K. Akbarzadeh-Sherbaf, B. Abdoli, S. Safari and A.-H. Vahabie, "A Scalable FPGA Architecture for Randomly Connected Networks of Hodgkin-Huxley Neurons," *Frontiers in Neuroscience*, vol. 12, 2018.
- [20] S. Y. Bonabi, H. Asgharian, S. Safari and M. N. Ahmadabadi, "FPGA implementation of a biological neural network based on the Hodgkin-Huxley neuron model," *Frontiers in Neuroscience*, vol. 8, 2014.
- [21] D.-A. Nguyen, X.-T. Tran and F. Iacopi, "A Review of Algorithms and Hardware Implementations for Spiking Neural Networks," *J. Low Power Electron. Appl.*, vol. 11, no. 2, 2021.
- [22] F. Akopyan, J. Sawada, A. Cassidy, R. Alvarez-Icaza, J. Arthur, P. Merolla, N. Imam, Y. Nakamura, P. Datta, G.-J. Nam, B. Taba, M. Beakes, B. Brezzo, J. B. Kuang, R. Manohar, W. P. Risk and B. Jackson, "TrueNorth: Design and Tool Flow of a 65 mW 1 Million Neuron Programmable Neurosynaptic Chip," *IEEE Transactions on Computer-Aided Design of Integrated Circuits and Systems*, vol. 34, no. 10, pp. 1537-1557, October 2015.
- [23] M. Sadeghi, Y. Rezaeiyan, D. F. Khatiboun, S. Eissa, F. Corradi, C. Augustine and F. Moradi, "NEXUS: A 28nm 3.3pJ/SOP 16-Core Spiking Neural Network With a Diamond Topology for Real-Time Data Processing," *IEEE Transactions on Biomedical Circuits and Systems*, vol. 19, no. 3, pp. 523-535, June 2025.
- [24] J. Han, Z. Li, W. Zheng and Y. Zhang, "Hardware Implementation of Spiking Neural Networks on FPGA," *Tsinghua Science and Technology*, vol. 25, no. 4, pp. 479-486, 2020.
- [25] S. Li, Z. Zhang, R. Mao, J. Xiao, L. Chang and J. Zhou, "A Fast and Energy-Efficient SNN Processor With Adaptive Clock/Event-Driven Computation Scheme and Online Learning," *IEEE Transactions on Circuits and Systems I: Regular Papers*, vol. 68, no. 4, pp. 1543-1552, 2021.
- [26] S. K. Lam, A. Pitrou and S. Seibert, "Numba: A LLVM-based Python JIT Compiler," in *Proceedings of the Second Workshop on the LLVM Compiler Infrastructure in HPC (LLVM '15)*, 2015.
- [27] S. Panchapakesan, Z. Fang and J. Li, "SyncNN: Evaluating and Accelerating Spiking Neural Networks on FPGAs," in *2021 31st International Conference on Field-Programmable Logic and Applications (FPL)*, 2021.
- [28] S. Gupta, A. Vyas and G. Trivedi, "FPGA Implementation of Simplified Spiking Neural Network," in *2020 27th IEEE International Conference on Electronics, Circuits and Systems*, 2020.
- [29] H. Liu, Y. Chen, Z. Zeng, M. Zhang and H. Qu, "A Low Power and Low Latency FPGA-Based Spiking Neural Network Accelerator," in *2023 International Joint Conference on Neural Networks (IJCNN)*, 2023.
- [30] A. Khodamoradi, K. Denolf and R. Kastner, "S2N2: A FPGA Accelerator for Streaming Spiking Neural Networks," in *The 2021 ACM/SIGDA International Symposium on Field-Programmable Gate Arrays (FPGA '21)*, New York, NY, USA, 2021.

-
- [31] A. Carpegna, A. Savino and S. D. Carlo, "Spiker: an FPGA-optimized Hardware accelerator for Spiking Neural Networks," 2022 IEEE Computer Society Annual Symposium on VLSI (ISVLSI), pp. 14-19, 2022.
 - [32] D. Gerlinghoff, Z. Wang, X. Gu, R. S. M. Goh and T. Luo, "E3NE: An End-to-End Framework for Accelerating Spiking Neural Networks With Emerging Neural Encoding on FPGAs," IEEE Transactions on Parallel and Distributed Systems, vol. 23, no. 11, pp. 233207-3219, 2022.
 - [33] J. Li, G. Shen, D. Zhao, Q. Zhang and Y. Zeng, "FireFly: A High-Throughput Hardware Accelerator for Spiking Neural Networks With Efficient DSP and Memory Optimization," IEEE Transactions on Very Large Scale Integration (VLSI) Systems, vol. 31, no. 8, pp. 1178-1191, 2023.
 - [34] Y. Nevarez, D. Rotermund, K. R. Pawelzik and A. Garcia-Ortiz, "Accelerating Spike-by-Spike Neural Networks on FPGA With Hybrid Custom Floating-Point and Logarithmic Dot-Product Approximation," IEEE Access, vol. 9, pp. 80603-80620, 2021.